Results in Physics 24 (2021) 104099

Contents lists available at ScienceDirect

Results in Physics

journal homepage: www.elsevier.com/locate/rinp

Developed selenium dioxide-based ceramics for advanced shielding applications: Au_2O_3 impact on nuclear radiation attenuation

Wiam Elshami [a], H.O. Tekin [a,b], M.S. Al-Buriahi [c], H.H. Hegazy [d,e], Mohamed M. Abuzaid [a], Shams A.M. Issa [f,g,*], M.H.M. Zaid [h,*], H.A.A. Sidek [h], K.A. Matori [h], Hesham M.H. Zakaly [g,i]

[a] Medical Diagnostic Imaging Department, College of Health Sciences, University of Sharjah, Sharjah, 27272, United Arab Emirates
[b] Uskudar University, Medical Radiation Research Center (USMERA), 34672 Istanbul, Turkey
[c] Department of Physics, Sakarya University, Sakarya, Turkey
[d] Research Center for Advanced Materials Science (RCAMS), King Khalid University, P. O. Box 9004, Abha 61413, Saudi Arabia
[e] Physics Dep., Faculty of Science, King Khalid University, P. O. Box 9004, Abha 61413, Saudi Arabia
[f] Physics Department, Faculty of Science, University of Tabuk, Tabuk 71451, Saudi Arabia
[g] Physics Department, Faculty of Science, Al-Azhar University, Assiut 71524, Egypt
[h] Department of Physics, University Putra Malaysia, 43400 Serdang, Selangor, Malaysia
[i] Institute of Physics and Technology, Ural Federal University, Ekaterinburg 620000, Russia

ARTICLE INFO

Keywords:
SeO_2-based ceramic
Buildup factor
Radiation
Shielding
Monte Carlo

ABSTRACT

The current research article aims to study the radiation shielding competence of a newly developed PbO-B_2O_3-SeO_2-Er_2O_3:Au_2O_3 glass ceramic. The concentrations of the constituent oxides were 40, 10, 49.5, and 0.5 mol % for PbO, B_2O_3, SeO_2, and Er_2O_3, respectively. The studied ceramic specimens were denoted by EA0, EA25, EA50, EA75 and EA100, and their density values were 5.87, 5.92, 5.94, 6.09, and 6.10 g/cm^3, respectively. The radiation shielding competence and photon buildup factors of the present ceramics were investigated under the Au_2O_3/SeO_2 substitution with ratio up to 0.1 mol %. The obtained results reveal that the MAC values were reported with 0.233 cm^2/g difference between the minimum and the maximum Au_2O_3 reinforced samples. The highest MAC values were reported for EA100 sample, which has the highest Au_2O_3 additive in its chemical structure. At 4 MeV photon energy, HVL values were reported as 3.2658 cm, 3.2352 cm, 3.2212 cm, 3.139 cm and 3.1309 cm for EA0, EA25, EA50, EA75 and EA100, respectively. Moreover, the highest values of EBF were observed for the EA100, and the lowest values of EBF were observed for EA0. Therefore, it can be concluded that the present ceramics possess high level shielding competence to use for various applications of gamma radiation.

Introduction

The use of ionizing radiation has been increased in the recent year in fields of medical industries. Exposure to ionizing radiation increases cancer risk, and radiation safety should be applied in all settings. ALARA principle, As Low As Reasonably Achievable, aims for radiation protection and implies increasing distance from radiation sources, reduction of exposure time and use of shielding [1]. Shielding is a common method to reduce radiation to us as it is not appropriate sometimes to reduce exposure time distance [2]. Concrete is a traditional method that used for radiation shielding. It is inexpensive It can be designed in many shapes and sizes. Nevertheless, it has many advantages, including thickness, opaqueness, occurrence of cracks due to exposure to high radiation and reduction in density and mechanical strength over time [3]. Lead glass provides an excellent option for radiation protection as it is not expensive and easy to fabricate. Nonetheless, it is not clearly transparent, has low strength and toxicity issues [4]. Therefore, many studies explored adding other heavy metals to improve properties of lead glasses [5–9]. Gold is a very rare heavy metal with high ductility and flexibility. It has high thermal and electrical conductivities. Gold is the most resistant metal to oxidation, but gold oxide (Au_2O_3) can be synthesized [10].Ag_2O in synthesized 40TeO_2-(60-y)V_2O_5-yAg_2O influence on the linear and nonlinear optical whaich revealed that the linear optical refractive index varied between 2.47 and 2.66 [11]. The glass sample (with no Ag_2O) has the lowest μ/ρ and can shield 50.3% of the photons at an energy of 0.284 MeV, while the glass sample has the

* Corresponding authors at: Physics Department, Faculty of Science, University of Tabuk, Tabuk 71451, Saudi Arabia (Shams A.M. Issa). Department of Physics, University Putra Malaysia, 43400, Serdang, Selangor, Malaysia. (M.H.M. Zaid).
E-mail addresses: shams_issa@yahoo.com (S.A.M. Issa), mhmzaid@upm.edu.my (M.H.M. Zaid).

https://doi.org/10.1016/j.rinp.2021.104099
Received 12 February 2021; Received in revised form 11 March 2021; Accepted 14 March 2021
Available online 22 March 2021

Table 1
Chemical compositions and densities for glass samples.

Code	B	O	Se	Er	Au	Pb	Density (g/cm^3)
EA0	0,010805	0,175907	0,390723	0,008359	0	0,414206	5,87
EA25	0,010773	0,175389	0,387607	0,008335	0,004907	0,412988	5,92
EA50	0,010742	0,174875	0,384509	0,00831	0,009786	0,411778	5,94
EA75	0,01071	0,174364	0,381429	0,008286	0,014636	0,410574	6,09
EA100	0,010679	0,173856	0,378367	0,008262	0,019458	0,409378	6,1

highest μ/ρ and can shield 78.5% of a beam of photons with the same energy. Greater Ag_2O content in the glasses, the lower TF, the more influential the radiation shield, and the possibility of being applied in several optical applications [12]. Use of gold in radiation protection might have a significant role as employing gold in radiotherapy showed that it decreases radiation dose to nearby [13]. Using the natural quartz of amethyst, chalcedony, crystal rock, milky, pink, flint, and jasper quartz in radiation protection might have a significant role as used in reactor building materials. These shielding features compared with those of the Portland concrete widely used as radiation shielding. In the low energy region where the photoelectric absorption is dominant, the mass interaction coefficients and the total linear attenuation coefficients have three resonances due to the Si, Ca, and Fe concentration; these resonances are also noticed in the effective atomic number. For photons below 60 keV, quartz's attenuation performance can be utilized for shielding of X-ray devices working with less than 60 kV, as reported in Marquez-Mata et al., 2021 [14]. On the other hand, Kavaz et al., 2020 [15] reported that barite and zirconolite increased the photon shielding potential of the glass-ceramics. Moreover, the insertion of SO_3 did not improve the neutron attenuation of the glass-ceramics. It can be inferred that barite and zirconolite additions to glass-ceramics improved the investigated samples' ability not only to shield from photons but also to neutrons and heavy charged particles [15]. This finding encourages the application of Au in the field of radiation protection. Therefore, it is important to assess feasibility of adding gold to shielding materials by evaluating the overall gamma ray attenuation properties. In this study, a group of $PbO\text{-}B_2O_3\text{-}SeO_2\text{-}Er_2O_3\text{:}Au_2O_3$ glass ceramics[16] was evaluated in terms of their gamma-ray shielding attenuation competencies. The investigated radiation attenuation parameters can be ordered as Linear attenuation coefficients (μ(E)), Mass attenuation coefficients (μ_m(E)), Effective electron density (N_{eff} (E)), Half value layer (HVL (E)), tenth value layer (TVL(E)) Exposure buildup factor (EBF (E)), and Energy absorption buildup factor (EABF (E)), as well as mean free path (mfp (E)), and Effective atomic number (Z_{eff} (E)). Moreover, effective atomic weight for absorption (A_{eff} (E)). against Photon energy (E) were also investigated. The outcomes from current investigation would be useful in understanding the direct impact of Au_2O_3 on gamma ray shielding competencies of studied glass structure.

Materials and methods

In this study, a group of glass-ceramics based on $PbO\text{-}B_2O_3\text{-}SeO_2\text{-}Er_2O_3\text{:}Au_2O_3$ system, which has been published by Siva Sesha Reddy [16] was evaluated in terms of their shielding competencies. Py-MLBUF software [17] and MCNPX [18]general-purpose Monte Carlo code. Investigated glass samples and their codes can be listed as below;

i) *EA0: $40PbO\text{-}10B_2O_3\text{-}49.5SeO_2\text{-}0.5Er_2O_3$*
ii) *EA25: $40PbO\text{-}10B_2O_3\text{-}49.25SeO_2\text{-}0.5Er_2O_3\text{:}0.025Au_2O_3$*
iii) *EA50: $40PbO\text{-}10B_2O_3\text{-}49.0SeO_2\text{-}0.5Er_2O_3\text{:}0.050Au_2O_3$*
iv) *EA75: $40PbO\text{-}10B_2O_3\text{-}48.75SeO_2\text{-}0.5Er_2O_3\text{:}0.075Au_2O_3$*
v) *EA100: $40PbO\text{-}10B_2O_3\text{-}48.50SeO_2\text{-}0.5Er_2O_3\text{:}0.1Au_2O_3$*

Shielding properties of studied glass samples

It is well-known that if an attenuator specimen as shield located between the detector and the source, intensity of incident gamma-ray reduces exponentially due to Beer-Lambert law [19,20]:

$$I = I_o e^{-\mu x} \quad (1)$$

I_o is the intensity of primary gamma, while I is the intensity of transmitted gamma through the glass. Besides, μ indicates the linear attenuation coefficient of the energy of interest. The term of × is the thickness of attenuator sample. In the case of a compound, the μ_m of glasses are estimated [21]:

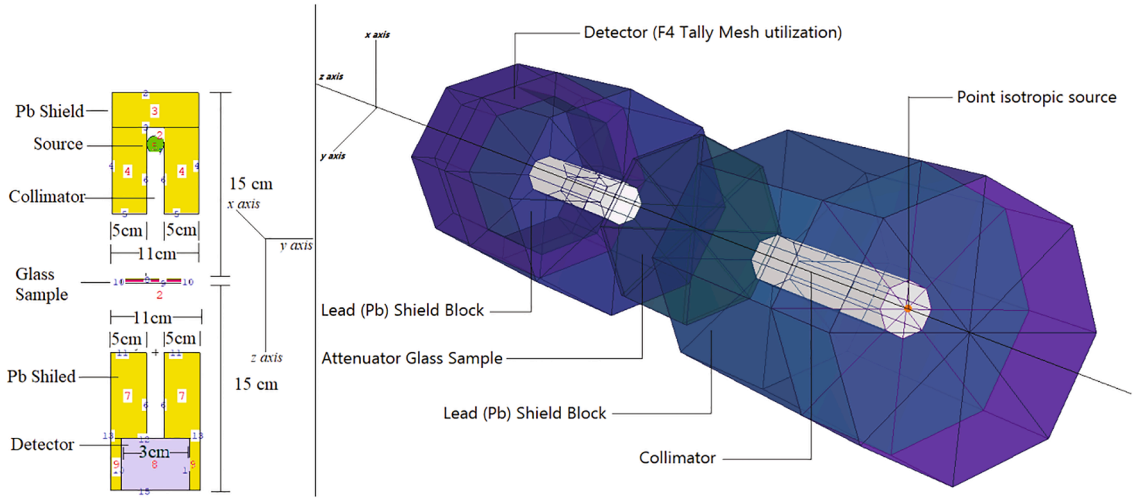

Fig. 1. MCNPX simulation setup for gamma-ray transmission studies (a) 2-D view with dimensions. (b) 3-D view of setup obtained from MCNPX Visual Editor.

Table 2
Mass attenuation coefficients (MAC) of studied glass samples obtained from **MCNPX** code and **Py-MLBUF** program.

	EA0		EA25		EA50		EA75		EA100	
Energy (MeV)	Py-MLBUF	MCNPX	Py-MLBUF	MCNPX	Py-MLBUF	MCNPX	Py-MLBUF	MCNPX	Py-MLBUF	MCNPX
0,015	87,8410	88,3254	88,1770	88,9251	88,5240	89,1254	88,8550	89,0125	89,2000	89,3254
0,02	55,1910	55,2652	55,3180	55,3225	55,4510	55,4624	55,5760	55,6124	55,7000	55,7425
0,0263	26,7670	26,9452	26,8310	26,9625	26,8980	26,9712	26,9610	26,9826	27,0000	26,9956
0,03	19,0120	19,1298	19,0590	19,1312	19,1080	19,1426	19,1540	19,1564	19,2000	19,2598
0,04	8,8720	8,9004	8,8951	8,9120	8,9190	8,9199	8,9417	8,9526	8,9600	8,9724
0,05	4,9189	4,9265	4,9323	4,9314	4,9461	4,9482	4,9592	4,9595	4,9700	4,9863
0,0595	3,2067	3,2109	3,2143	3,2154	3,2233	3,2258	3,2318	3,2326	3,2400	3,2486
0,06	3,1436	3,1442	3,1510	3,1512	3,1598	3,1601	3,1682	3,1698	3,1800	3,1824
0,08	1,5134	1,5142	1,5171	1,5184	1,5214	1,5219	1,5255	1,5264	1,5300	1,5358
0,1	2,6029	2,6124	2,6192	2,6214	2,6357	2,6362	2,6518	2,6524	2,6700	2,6824
0,15	0,9763	0,9801	0,9819	0,9821	0,9877	0,9881	0,9933	0,9951	0,9990	1,0091
0,2	0,5101	0,5126	0,5127	0,5131	0,5154	0,5162	0,5180	0,5192	0,5210	0,5216
0,3	0,2339	0,2342	0,2348	0,2350	0,2357	0,2360	0,2366	0,2371	0,2380	0,2385
0,4	0,1517	0,1519	0,1522	0,1523	0,1526	0,1529	0,1530	0,1541	0,1530	0,1543
0,5	0,1158	0,1161	0,1161	0,1162	0,1163	0,1165	0,1166	0,1174	0,1170	0,1178
0,6	0,0962	0,0973	0,0964	0,0978	0,0966	0,0969	0,0967	0,0971	0,0969	0,0973
0,662	0,0879	0,0881	0,0880	0,0882	0,0882	0,0885	0,0883	0,0886	0,0884	0,0888
0,8	0,0752	0,0763	0,0753	0,0765	0,0754	0,0767	0,0754	0,0769	0,0755	0,0771
1	0,0637	0,0642	0,0638	0,0644	0,0638	0,0645	0,0639	0,0648	0,0639	0,0649
1,173	0,0572	0,0578	0,0572	0,0579	0,0573	0,0581	0,0573	0,0584	0,0573	0,0586
1,333	0,0528	0,0534	0,0528	0,0536	0,0529	0,0538	0,0529	0,0542	0,0529	0,0545
1,5	0,0495	0,0498	0,0495	0,0499	0,0495	0,0506	0,0496	0,0518	0,0496	0,0520
2	0,0434	0,0436	0,0434	0,0438	0,0434	0,0439	0,0435	0,0443	0,0435	0,0445
2,506	0,0401	0,0412	0,0401	0,0414	0,0401	0,0415	0,0401	0,0417	0,0402	0,0419
3	0,0381	0,0385	0,0382	0,0386	0,0382	0,0388	0,0382	0,0395	0,0382	0,0398
4	0,0362	0,0365	0,0362	0,0367	0,0362	0,0369	0,0363	0,0372	0,0363	0,0375
5	0,0355	0,0358	0,0355	0,0359	0,0356	0,0361	0,0356	0,0365	0,0356	0,0366
6	0,0354	0,0356	0,0354	0,0358	0,0355	0,0359	0,0355	0,0362	0,0356	0,0363
8	0,0361	0,0363	0,0362	0,0365	0,0362	0,0367	0,0363	0,0369	0,0363	0,0370
10	0,0373	0,0375	0,0374	0,0377	0,0374	0,0378	0,0375	0,0381	0,0376	0,0385
15	0,0406	0,0412	0,0407	0,0413	0,0408	0,0415	0,0408	0,0417	0,0409	0,0419

$$MAC = \sum_i w_i (MAC)_i \tag{2}$$

where w_i is the weight fraction of the i^{th} constitute elements.

The effective atomic number and effective electron density, depending on the total molecular cross-section (σ_t), total atomic cross-section (σ_a) and total electronic cross-section (σ_e), was used to measure the total effective atomic cross-section [22].

$$\sigma_t = \frac{1}{N_A}\sum_i n_i A_i (MAC)_i \tag{3}$$

$$\sigma_a = \frac{1}{N_A}\sum_i f_i A_i (MAC)_i \tag{4}$$

$$\sigma_e = \frac{1}{N_A}\sum_i \frac{f_i A_i}{Z_i} (MAC)_i \tag{5}$$

$$Z_{eff} = \frac{\sigma_a}{\sigma_e} \tag{6}$$

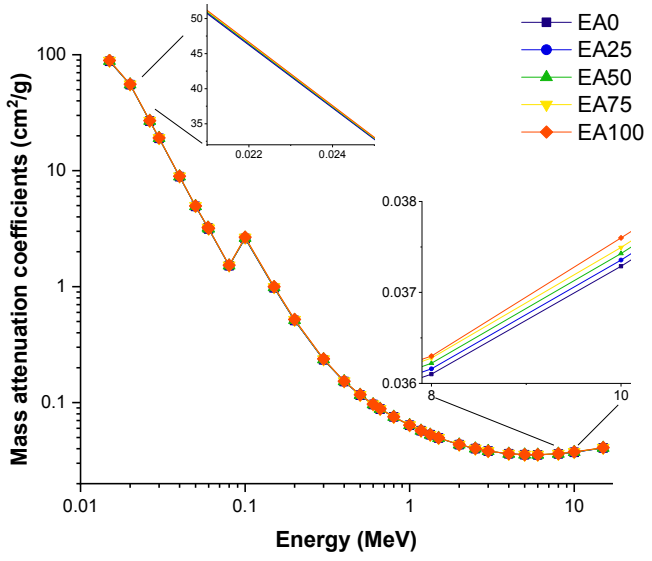

Fig. 2. Variation of mass attenuation coefficients against Photon energy (E) for all glasses.

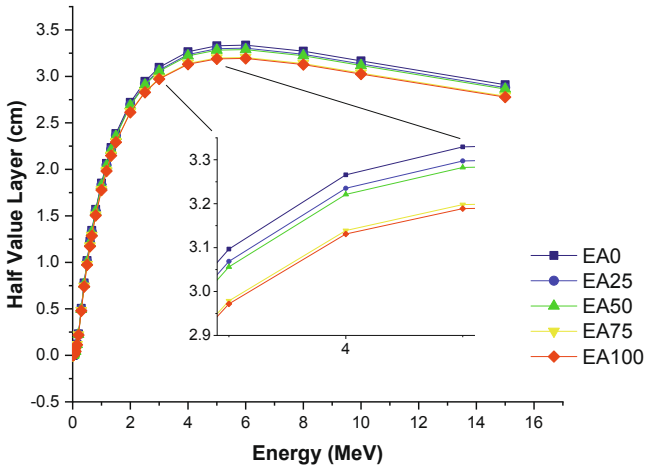

Fig. 3. Variation of half value layer (HVL) against Photon energy for all glasses.

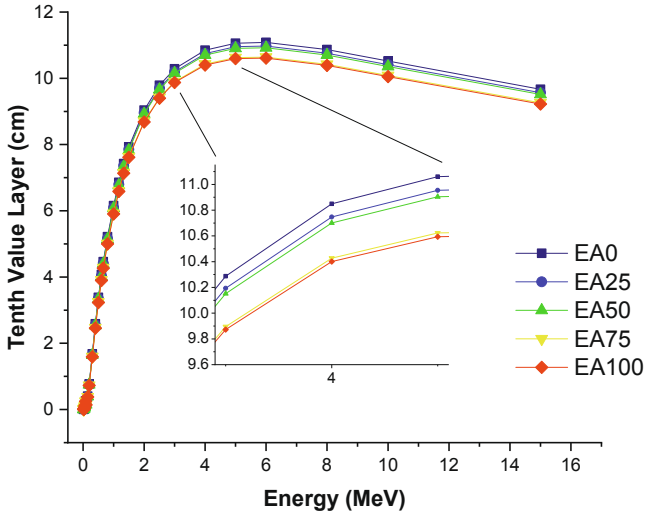

Fig. 4. Variation of tenth value layer (TVL) against Photon energy for all glasses.

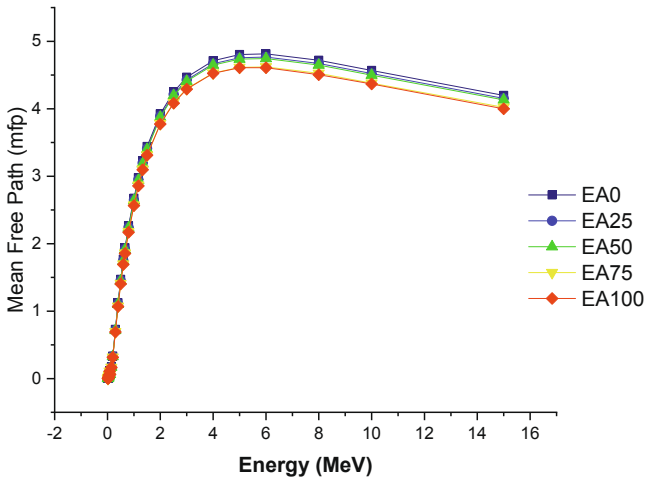

Fig. 5. Variation of men free path (λ) against Photon energy for all glasses.

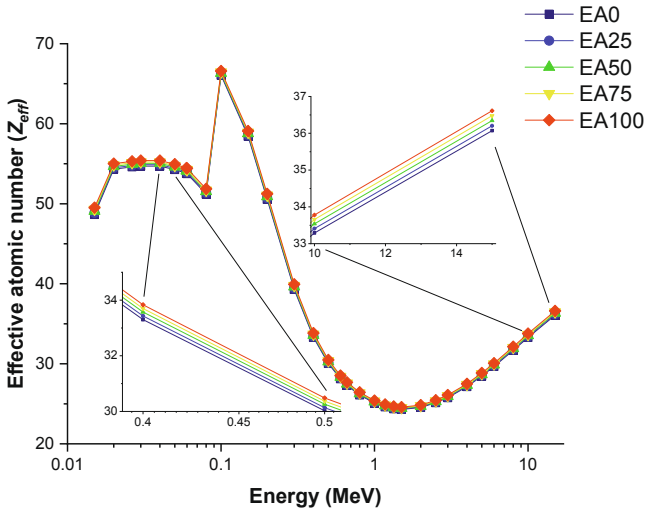

Fig. 6. Variation of effective atomic number (Z_{eff}) against Photon energy for all glasses.

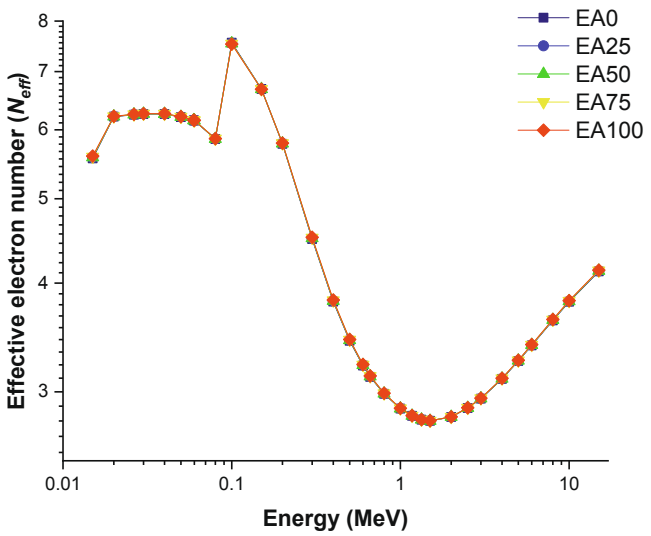

Fig. 7. Variation of effective electron number (N_{eff}) against Photon energy for all glasses.

$$N_{eff} = \frac{(MAC)}{\sigma_e} \tag{7}$$

The terms of n_i, A_i, Z_i, f_i and N_A are the number of atoms, atomic weight, atomic number, fractional abundance of i^{th} element and Avogadro number. The shielding thickness that decreases by 1/2 the intensity of incident radiation is called the half-value layer (HVL), that is calculated by equation (8) [23,24]:

$$HVL = \frac{\ln(2)}{LAC} \tag{8}$$

An absorption of 0.368 of the incident gamma radiation was observed by materials that have a thickness of one mean free path[25]:

$$MFP = \frac{1}{LAC} \tag{9}$$

Where LAC is the liner attenuation coefficient. The exposure buildup factor and energy absorption buildup factor terms are also key parameters for seeing overall contributions to the attenuation of gamma rays in material. Geometry-Progressive (G-P) approach was used to evaluate exposure buildup factor and energy absorption buildup factor, in the analysis. The details of aforementioned method can be found in literature elsewhere [26–29].

Simulation studies using MCNPX general purpose Monte Carlo code (v. 2.7.0)

Different versions of MCNP code have been widely used to estimate the photon transmission through several shielding materials[30–33]. MCNPX general-purpose Monte Carlo code was implemented for gamma-ray transmission simulations of different glassy systems. Previously, version 2.7.0 of MCNPX code was used for investigation of different types of shielding materials [26–29]. Accordingly, mass attenuation coefficients $\mu_m(E)$ of PbO-B_2O_3-SeO_2-Er_2O_3:Au_2O_3 glass system were determined at 0.015–15 MeV photon energy range. The essential parts of INPUT file such as cell cards and surface cards were prepared using elemental mass fractions (%wt.) and material densities [see Table 1] as well as geometrical locations of equipment in simulation environment. Next, $\mu_m(E)$ values obtained from Py-MLBUF [17] and MCNPX [18] were compared. It's worth mentioning that obtained results were reported with well accordance. Somehow, minor numerical differences were observed between Py-MLBUF and the Monte Carlo code. The small "minor" deviations in mass attenuation coefficient

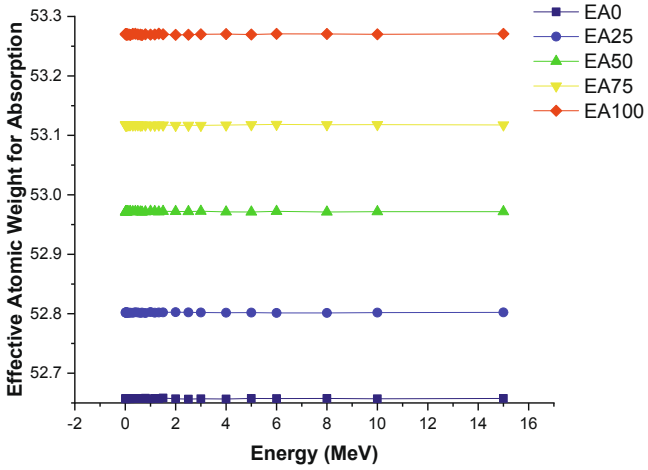

Fig. 8. Variation of effective atomic weight for absorption against Photon energy for all glasses.

quantities deduced by computational and theoretical methods could commonly take place due to slight variations in considered mathematical and physical models, geometry and ambiguities in the atomic data for each method. whereas Py-MLBUF is a mechanism that utilizes mathematical improvement for direct determination of μ_m(E). For the MCNPX, there is no direct method to obtain μ_m(E) values. It requires some sub-steps such as exporting of attenuated gamma-ray flux quantity from detector and accordingly utilization of Beer-Lambert Law (see equation (1)). In the MCNPX input file, the glass samples were defined in terms of their elemental mass fractions (weight per unit length), and dimensions (cm). The gamma-ray emitting systems' total geometry can be seen in Fig. 1. In Fig. 1 is shown the Monte Carlo model including the radiation source, the cell defining the detector, and the shielding material. A hollow-detection cell was defined by using F4 tally mesh. This type of tally mesh provides an average photon flux in a point or cell. Therefore, total photon flux in hollow-detection cell was measured. The simulation phase was repeated from 0.015 to 15 MeV for each glass sample, respectively. In addition, some of the variance reduction methods were used. For example, to optimize productivity by simulation, neutron and electron tracking were switched off, and only photon tracking was enabled in cell description. Finally, attenuated photon flux has been counted in F4 Tally Mesh detection field to count the number of photons entering the detector per MeVcm^{2}s^{-1}. The test of the recent MCNPX simulation has been implemented by using the D00205ALLCP03 MCNPXDATA package is included of DLC-200/MCNPDATA cross-section libraries. The number of histories (NPS variable) used in the MCNPX simulation was set as 10^8. It's worth mentioning that energy cutoff was set for 0.001 MeV, which means that photons below 0.001 MeV has not been considered in terms of tracking (Table 2).

Results and discussions

In this study, five different glasses encoded EA0, EA25, EA50, EA75 and EA100 based PbO-B_2O_3-SeO_2-Er_2O_3:Au_2O_3 system were investigated in terms of their attenuation properties against ionizing gamma-rays. The densities of the glasses were reported as 5.87 g/cm^3, 5.92 g/cm3, 5.94 g/cm^3, 6.09 g/cm^3, 6.10 g/cm^3 for EA0, EA25, EA50, EA75 and EA100, respectively. Firstly, mass attenuation coefficients of studied glasses were determined in a wide range photon energy (i.e. 0.015 MeV-15 MeV). For any material the total mass interaction coefficient defines the shielding features independent of the degree of agglomeration of the matter. Fig. 2 shows the variation of μ_m versus photon capacity (E). By observing the gamma-ray radiation and chemical composition of the glasses, one can infer how different the variations of μ_m(E) values have been. It shows systematic differences among the studied glasses across three distinct regions such as low, middle and high energy regions. In the low-energy region, where photoelectric (PE) is the dominant mechanism, a steep drop was observed. Compton Scattering shows major changes in terms of μ_m(E). It was an obvious interference from the Fig. 2 that μ_m(E) values decreased with increasing photon energy. This can be explained by dependence of μ in the Beer-Lambert law (see Equation (1)). However, slight differences between the studied glasses in three basic energy region were also reported. The increasing Au_2O_3 additive increased the μ_m(E) values systematically. This situation can be explained more comprehensively by looking at the low energy regions of Fig. 2. The μ_m(E) values are decreased almost linearly between 0.022 and 0.024 MeV. However, the highest μ_m(E) values were reported for EA100 sample, which has the highest Au_2O_3 additive in its chemical structure. For example, μ_m(E) values were reported as 26.7670 cm^2/g, 26.8310 cm^2/g, 26.8980 cm^2/g, 26.9610 cm^2/g, 27.0000 cm^2/g at 0.026 MeV for EA0, EA25, EA50, EA75 and EA100, respectively. The μ_m(E) values were reported with 0.233 cm^2/g difference between the minimum and the maximum Au_2O_3 reinforced samples. Similarly, this situation was also reported in high energy zone. The μ_m(E) values were reported in similar upward trend from EA0 to EA100. The reported MAC are ordered as 0.0361, 0.0362, 0.036, 0.0363, 0.0363 at 8 MeV for EA0, EA25, EA50, EA75 and EA100, respectively. The similar results were reported in literature [34–40], where the reinforcement with higher atomic numbers has increased the μ_m(E) values against incident photons. The shielding material's gamma attenuation is significant, along with its HVL(E) transmission factor [41]. The findings of the investigation of the glass pieces are shown in Fig. 3. It is well-known that lower HVL(E) values are the pattern of superior shielding properties among the investigated shielding materials. This can be explained by the nature of HVL(E), which has an inverse relationship with linear attenuation coefficient (μ) [42–44]. Therefore, once can say that samples with higher μ values shall provide lower HVL(E) values. Fig. 3 depicts the variation of half value layer HVL(E) against photon energy for all glasses. Among the investigated glasses, EA100 sample was reported with its lowest HVL(E) values at all individual photon energies. This situation can be explained in parallel of μ_m(E) values, where the EA100 sample showed superior behaviors. At 4 MeV photon energy, HVL (E) values were reported as 3.2658 cm, 3.2352 cm, 3.2212 cm, 3.139 cm and 3.1309 cm for EA0, EA25, EA50, EA75 and EA100, respectively. If we consider it from another perspective, the difference of HVL(E) values was reported as 0.1043 cm at 4 MeV. One can say that EA100 sample requires 0.1043 cm less material thickness at 4 MeV to reduce the intensity of incident photons to its half. Similarly, HVL(E) values of studied glasses can be listed as 2.9102 cm, 2.8795 cm, 2.8634 cm, 2.787 cm, 2.7765 at 15 MeV

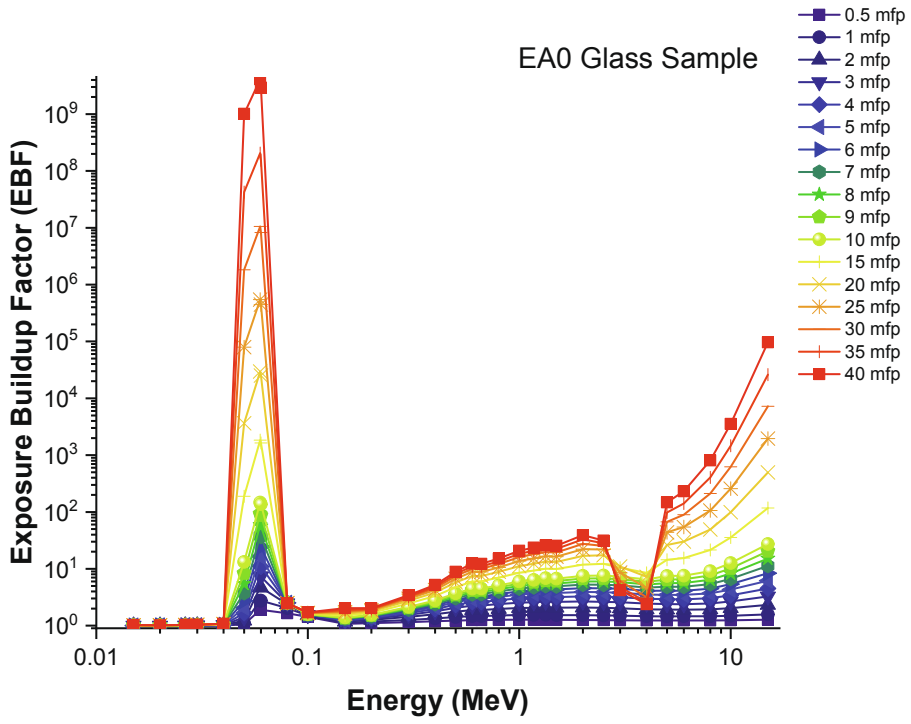

(a)

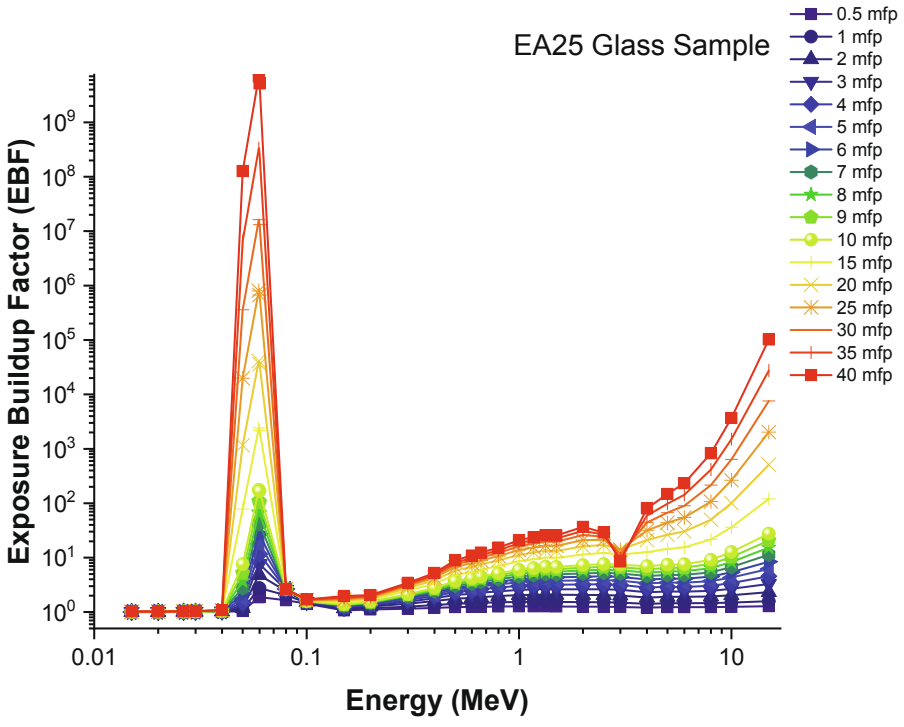

(b)

Fig. 9. (a-e) Variation of exposure buildup factor (EBF) against Photon energy for all glasses.

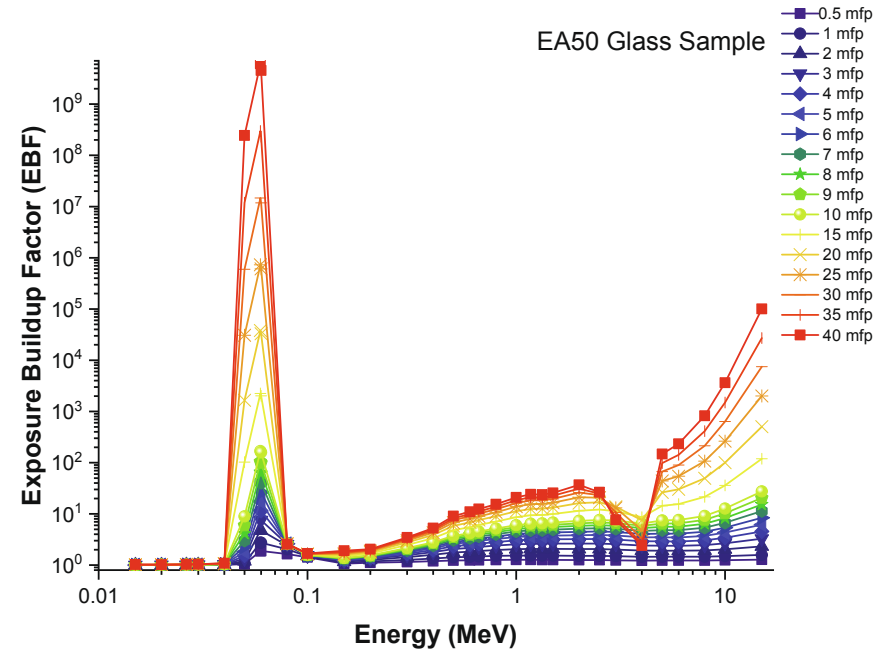

(c)

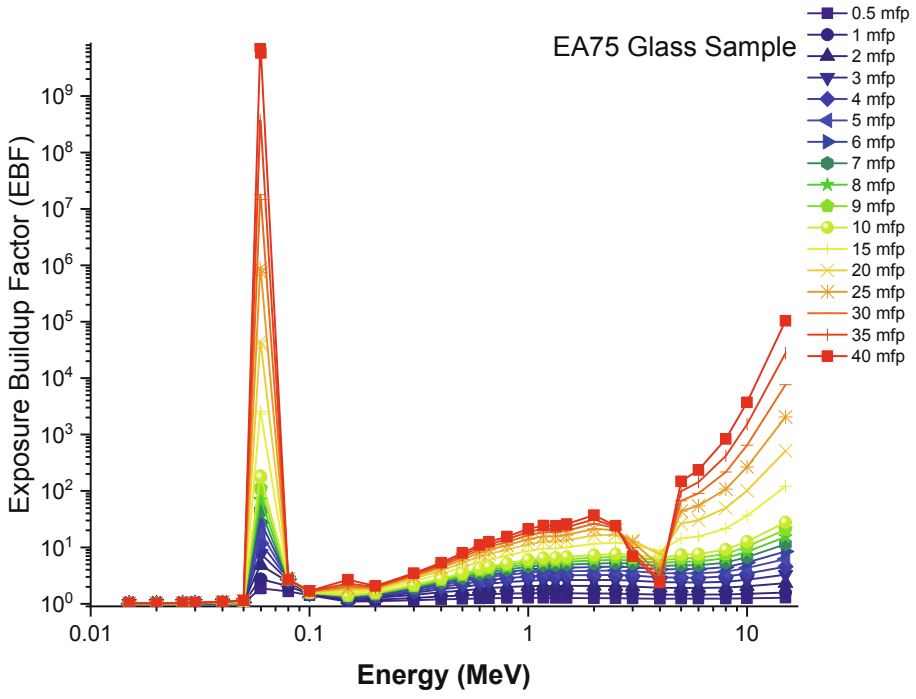

(d)

Fig. 9. (*continued*).

photon energy, which is the maximum photon energy of the current investigation. The quantitative difference between the first and last sample (i.e. EA0 and EA100) is 0.1317 cm. Therefore, a remarkable inference can be highlighted by attenuation superiority of EA100 sample is relatively higher at higher energies. Another shielding feature for materials can be explained by tenth value layer, which is the required thickness to reduce primary gamma ray intensity to its one tenth. Similar to HVL thickness, TVL is also a useful tool for overall evaluation of shields in terms of required fabrication sizes in specific energies. Fig. 4 shows the variation of tenth value layer TVL(E) against photon energy for all glasses. The changing trend in HVL(E) was also reported for TVL (E) values at 0.015 MeV-15 MeV photon energy range. The minimum values were reported for EA100 sample. At 15 MeV photon energy, TVL (E) values were reported as 9.6675 cm, 9.5654 cm, 9.5121 cm, 9.2582 cm and 9.2233 cm for EA0, EA25, EA50, EA75 and EA100, respectively. While the Au amount in the glass samples increased from 0 to 0.019458

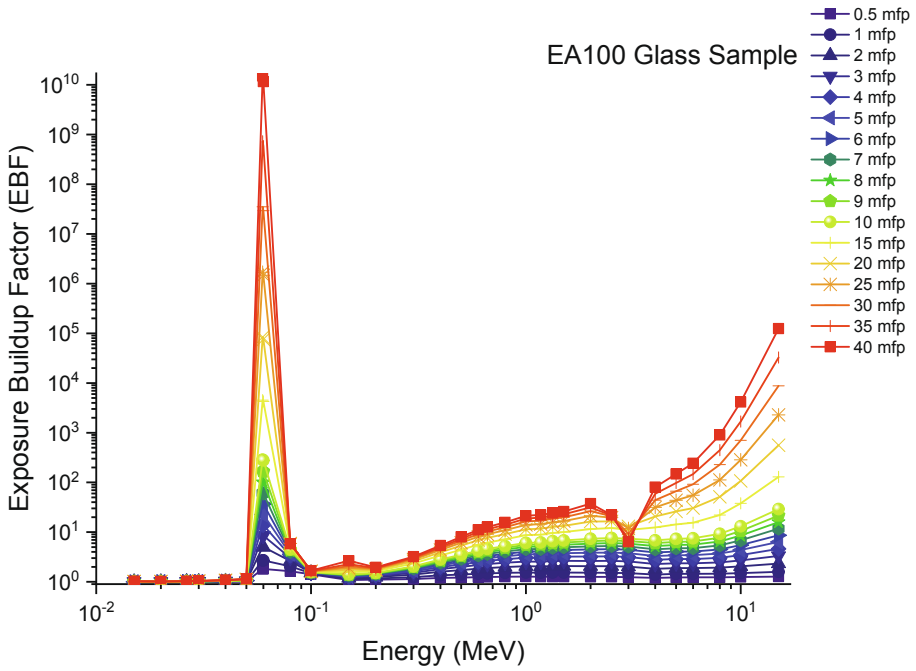

(e)

Fig. 9. (*continued*).

wt%, TVL(E) values decreased from 9.6675 cm to 9.2582 cm. The quantitative difference was reported as 0.4093 cm. The term of mean free path (often referred as mfp(E)) is also a parameter in gamma-protection competencies of candidate shielding materials. The glass samples were evaluated in terms of mean free path values, and the findings are presented in Fig. 5. The reported behaviors of mfp(E) values usually vary similar to the changing trend of HVL(E). The lower average mfp(E) values for the EA100 glass were also reported in summary. The term of effective atomic number (Z_{eff}) for evaluating the appropriateness of the substance for gamma applications is associated with the appropriate partial photon mitigation step. Fig. 6 depicts variation of effective atomic number Z_{eff} (E) against photon energy for all glasses. The maximum effective atomic number values such as 66.0604, 66.1928, 66.3285, 66.4567, 66.5838 were reported at 0.03 MeV photon energy for EA0, EA25, EA50, EA75 and EA100 samples, respectively. This is an evidence that partial photon mitigation of increasing high atomic number additives such as Au increased the effective Z number of EA100 sample, where the direct contribution of Au_2O_3 reinforcement was obvious. The term of effective electron number (N_{eff}) for gamma ray shielding applications can be considered as another important feature of composite materials for partial photon mitigation step. The relationship between the atomic number and electron number is directly related with effective electron numbers of materials against incoming photons. Fig. 7 shows changes in effective electron numbers N_{eff}(E) against photon energy for all glasses. In parallel to situation effective atomic number, the highest effective electron number values were also reported for EA100 sample, which has the highest Au amount in its structure. The term of effective atomic weight (A_{eff}) of a substance varies from product to product. This idea emphasizes the atomic weight interaction process and what occurs in terms of absorption process [45]. Likely similar to Z_{eff} and N_{eff}, a single value A_{eff} of a complex material's atomic weight may represent a sum may be viewed as a possible explanation for effective density. This activity inspired us to comprehend the radiative interaction, which enhanced our ability to appreciate the atomic weight mechanism. A total can be found by looking at the number of nucleons, which has to collide with particles in the nucleus. In this study, A_{eff} values of studied glasses were also reported using Py-MLBUF software. Fig. 8 shows the variation of A_{eff} (E) against photon energy for all glasses. The results showed that there is an increment in A_{eff} (E) values with increasing Au_2O_3 additive in glass compositions. The A_{eff} (E) values were reported as 52.6576 g/mole, 52.8023 g/mole, 52.9717 g/mole,53.1175 g/mole, 53.2707 g/mole for EA0, EA25, EA50, EA75 and EA100 samples, respectively. As it can be seen from the quantities, there was no sharp differences between the EA0 and EA100. This can be explained with the slight increments in Au_2O_3 additive, which has also slightly affected the effective atomic weight for absorption from EA0 to EA. Fig. 9 (a-e) shows the variation of exposure buildup factor EBF(E) as a function the energy (up to 15 MeV) at various depths (up to 40 mfp) for EA0, EA25, EA50, EA75 and EA100 samples, respectively. The lowest EBF(E) was at the low and high photon energy levels. In comparison, the highest EBF(E) was at the medium photon energy. This kind of action is the product of the absorption processes (e.g. photoelectric at low energy region and pair production and high one). However, the higher levels of energy above the Compton range play a critical role in rising the EBF(E). Furthermore, it is clear that the highest values of EBF were observed for the EA100, and the lowest values EBF(E) were observed for EA0. Fig. 10 (a-e) illustrates the variation of energy absorption buildup factor EABF (E) as a function the energy (up to 15 MeV) at various depths (up to 40 mfp) for EA0, EA25, EA50, EA75 and EA100 samples, respectively. The behavior of EABF(E) values seem similar to those of EBF(E). However, the EABF(E) values are bigger than those of EBF(E) especially at the low and high energy regions due to the dominant of the absorption processes (e.g. photoelectric at low energy region and pair production and high one). The actions of EABF(E) and EBF(E) are identical. However, the EABF(E) values are greater at lower and higher energies, owing to the dominant processes at these energy levels (e.g. photoelectric at low energy region and pair production and high one).

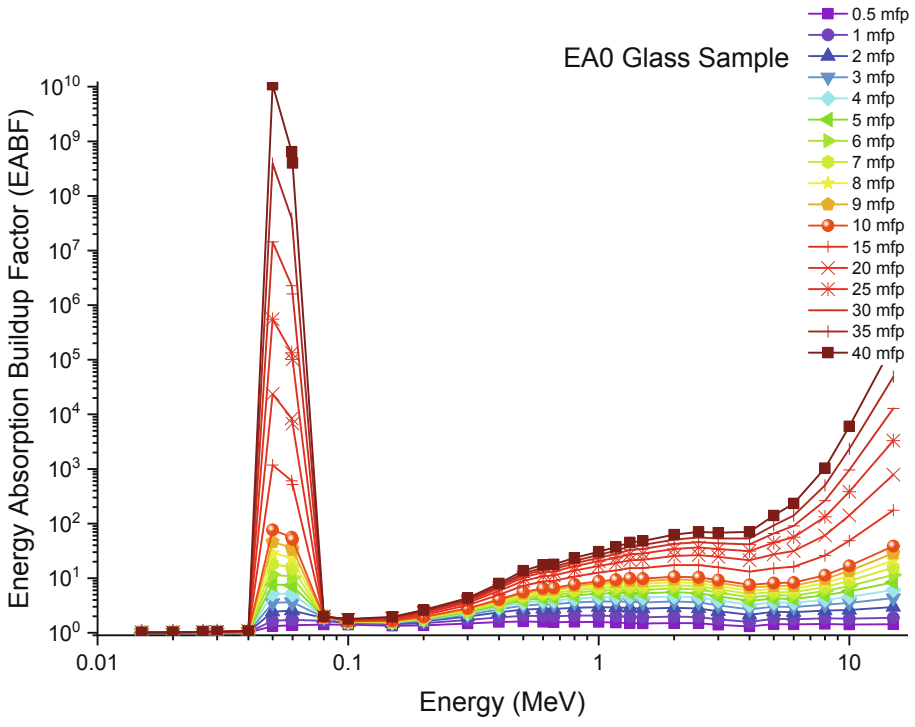

(a)

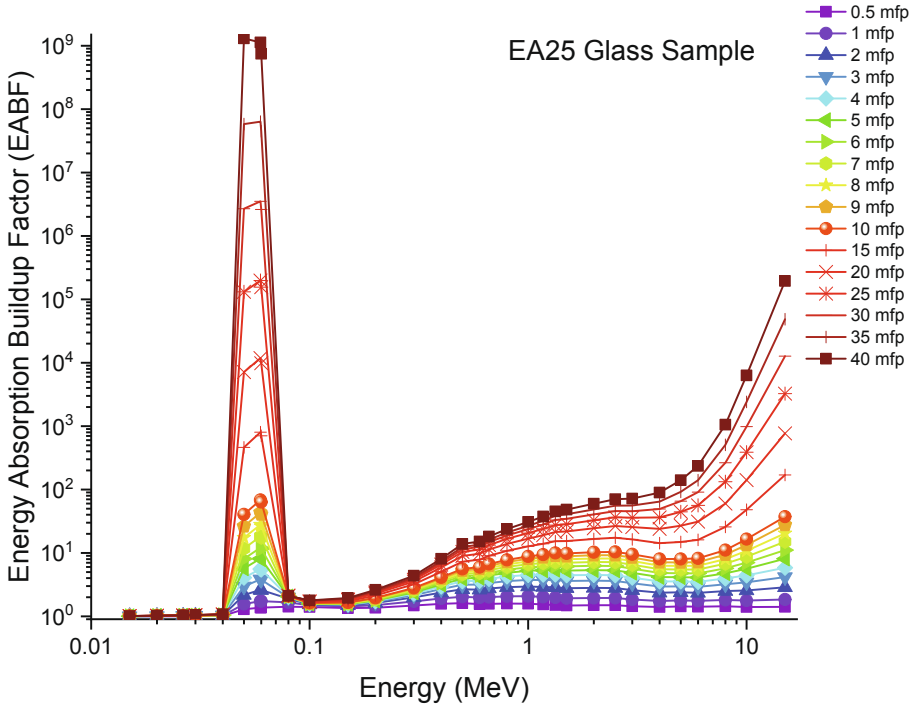

(b)

Fig. 10. (a-e) Variation of energy absorption buildup factor (EABF) against Photon energy for all glasses.

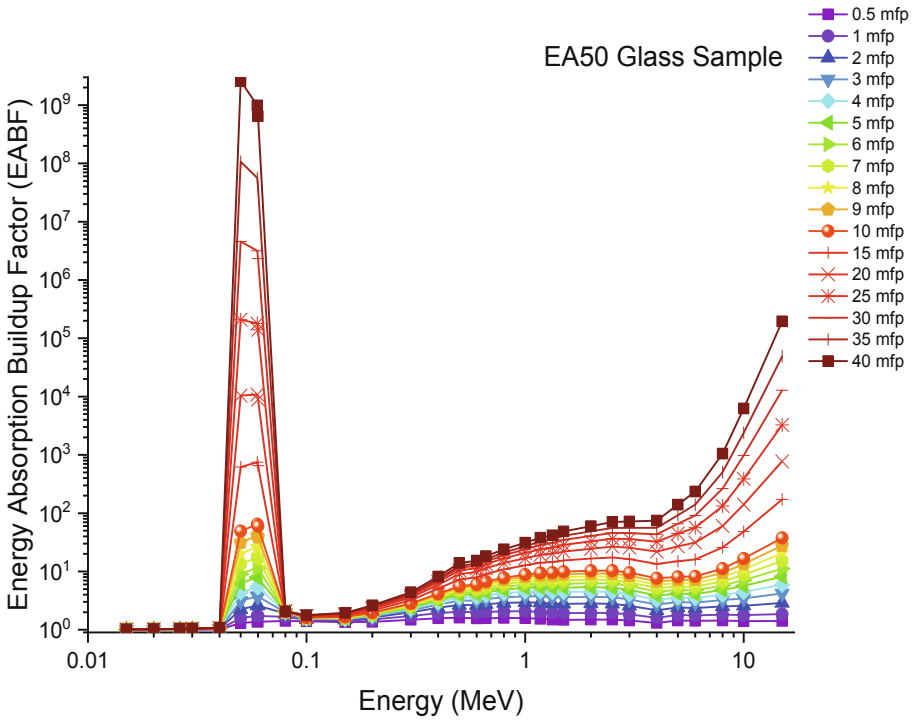

(c)

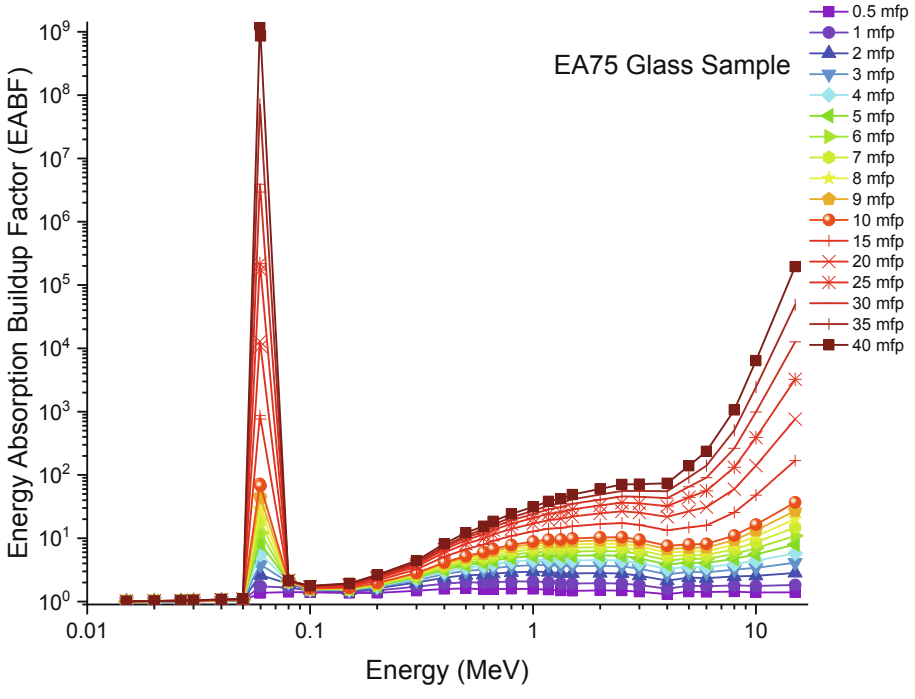

(d)

Fig. 10. (*continued*).

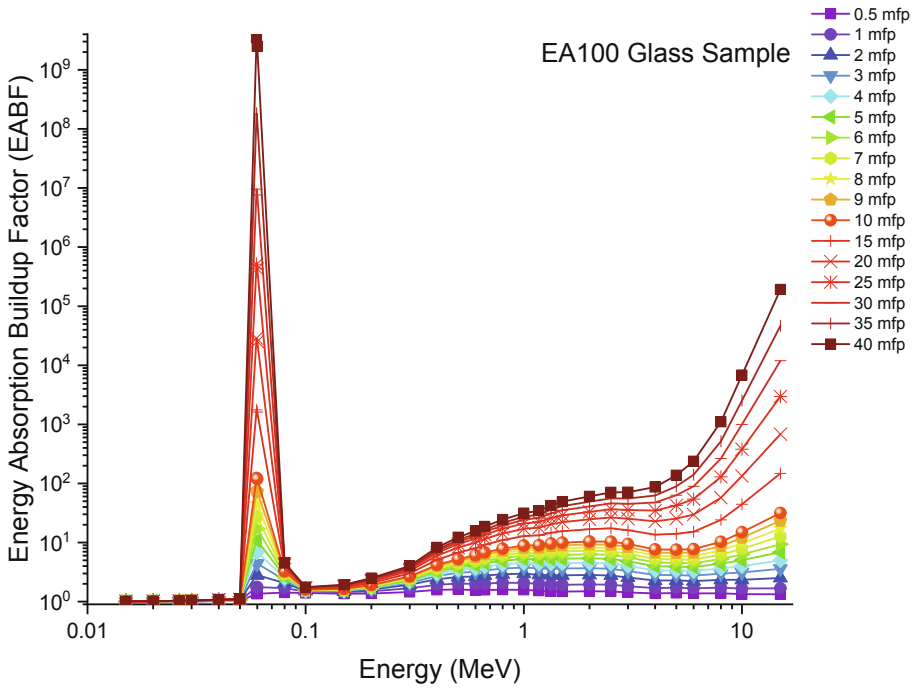

(e)

Fig. 10. (*continued*).

Conclusion

The current research article reported on the radiation shielding competence of a newly developed PbO-B_2O_3-SeO_2-Er_2O_3:Au_2O_3 glass ceramic. The studied ceramic specimens were denoted by EA0, EA25, EA50, EA75 and EA100, and their density values were 5.87, 5.92, 5.94, 6.09, and 6.10 g/cm^3, respectively. The radiation shielding competence and photon buildup factors of the present ceramics were investigated under the Au_2O_3/SeO_2 substitution with ratio up to 0.1 mol%. We found that the MAC values were reported with 0.233 cm^2/g difference between the minimum and the maximum Au_2O_3 reinforced samples. The highest MAC values were reported for EA100 sample, which has the highest Au_2O_3 additive in its chemical structure. At 15 MeV photon energy, TVL values were reported as 9.6675 cm, 9.5654 cm, 9.5121 cm, 9.2582 cm and 9.2233 cm for EA0, EA25, EA50, EA75 and EA100, respectively. The maximum effective atomic number values such as 66.0604, 66.1928, 66.3285, 66.4567, 66.5838 were reported at 0.03 MeV photon energy for EA0, EA25, EA50, EA75 and EA100 samples, respectively. Furthermore, there is an increment in A_{eff} values with increasing Au_2O_3 additive in glass compositions. The A_{eff} values were reported as 52.6576 g/mole, 52.8023 g/mole, 52.9717 g/mole, 53.1175 g/mole, 53.2707 g/mole for EA0, EA25, EA50, EA75 and EA100 samples, respectively. Moreover, the highest values of EBF were observed for the EA100, and the lowest values of EBF were observed for EA0. Therefore, it can be concluded that the present ceramics possess high level shielding competence to use for various applications of gamma radiation.

CRediT authorship contribution statement

Wiam Elshami: Conceptualization, Investigation, Writing - original draft. **H.O. Tekin:** Conceptualization, Investigation, Methodology, Writing - original draft. **M.S. Al-Buriahi:** Writing - original draft, Investigation, Methodology, Conceptualization. **H.H. Hegazy:** Conceptualization, Investigation, Methodology, Supervision, Writing - review & editing. **Mohamed M. Abuzaid:** Investigation, Supervision, Writing - original draft, Writing - review & editing. **Shams A.M. Issa:** Investigation, Conceptualization, Supervision, Writing - review & editing. **M.H.M. Zaid:** Investigation, Conceptualization, Funding acquisition, Supervision, Writing - review & editing. **H.A.A. Sidek:** Investigation, Conceptualization, Supervision, Writing - review & editing. **K.A. Matori:** Investigation, Conceptualization, Supervision, Writing - review & editing. **Hesham M.H. Zakaly:** Investigation, Methodology, Supervision, Writing - original draft.

Declaration of Competing Interest

The authors declare that they have no known competing financial interests or personal relationships that could have appeared to influence the work reported in this paper.

Acknowledgement

The authors extend their appreciation to the Deanship of Scientific Research at King Khalid University for the financial support through research groups program under grant number (R.G.P2/98/41).

References

[1] I.C.R.P. International commission on radiological protection. Acta Radiol 1954;41:708–12. https://doi.org/10.3109/00016925409177277.
[2] Elshami W, Abuzaid MM, Tekin HO. Effectiveness of breast and eye shielding during cervical spine radiography: An experimental study. Risk Manag Healthc Policy 2020;13:697–704. https://doi.org/10.2147/RMHP.S257185.
[3] Lakshminarayana G, Baki SO, Kaky KM, Sayyed MI, Tekin HO, Lira A, Kityk IV, Mahdi MA. Investigation of structural, thermal properties and shielding parameters for multicomponent borate glasses for gamma and neutron radiation shielding applications. J Non-Cryst Solids 2017;471:222–37. https://doi.org/10.1016/j.jnoncrysol.2017.06.001.
[4] Scuderi GJ, Brusovanik GV, Campbell DR, Henry RP, Kwon B, Vaccaro AR. Evaluation of non–lead-based protective radiological material in spinal surgery. Spine J. 2006;6(5):577–82. https://doi.org/10.1016/j.spinee.2005.09.010.
[5] Tekin HO, Kilicoglu O, Kavaz E, Altunsoy EE, Almatari M, Agar O, Sayyed MI. The investigation of gamma-ray and neutron shielding parameters of Na2O-CaO-P2O5-SiO2 bioactive glasses using MCNPX code. Results Phys 2019;12:1797–804. https://doi.org/10.1016/j.rinp.2019.02.017.

[6] Uosif MAM, Mostafa AMA, Issa SAM, Tekin HO, Alrowaili ZA, Kilicoglu O. Structural, mechanical and radiation shielding properties of newly developed tungsten lithium borate glasses: An experimental study. J Non-Cryst Solids 2020; 532:119882. https://doi.org/10.1016/j.jnoncrysol.2019.119882.
[7] Tekin HO, Altunsoy EE, Kavaz E, Sayyed MI, Agar O, Kamislioglu M. Photon and neutron shielding performance of boron phosphate glasses for diagnostic radiology facilities. Results Phys 2019;12:1457–64. https://doi.org/10.1016/j.rinp.2019.01.060.
[8] Dong MG, Agar O, Tekin HO, Kilicoglu O, Kaky KM, Sayyed MI. A comparative study on gamma photon shielding features of various germanate glass systems. Compos B Eng 2019;165:636–47. https://doi.org/10.1016/j.compositesb.2019.02.022.
[9] Rammah YS, Sayyed MI, Ali AA, Tekin HO, El-Mallawany R. Optical properties and gamma-shielding features of bismuth borate glasses. Appl. Phys. A 2018;124(12). https://doi.org/10.1007/s00339-018-2252-7.
[10] Shi H, Asahi R, Stampfl C. Properties of the gold oxides Au2 O3 and Au2 O: First-principles investigation. Phys Rev B - Condens Matter Mater Phys 2007;75:205125. https://doi.org/10.1103/PhysRevB.75.205125.
[11] Sayyed MI, Rashad M, Rammah YS. Impact of Ag2O on linear, nonlinear optical and gamma-ray shielding features of ternary silver vanadio-tellurite glasses: TeO2–V2O5–Ag2O. Ceram Int 2020;46(14):22964–72. https://doi.org/10.1016/j.ceramint.2020.06.071.
[12] Al-Buriahi MS, Singh VP, Alalawi A, Sriwunkum C, Tonguc BT. Mechanical features and radiation shielding properties of TeO2–Ag2O-WO3 glasses. Ceram Int 2020;46(10):15464–72. https://doi.org/10.1016/j.ceramint.2020.03.091.
[13] Brivio D, Nguyen PL, Sajo E, Ngwa W, Zygmanski P. A Monte Carlo study of I-125 prostate brachytherapy with gold nanoparticles: dose enhancement with simultaneous rectal dose sparing via radiation shielding. Phys. Med. Biol. 2017;62(5):1935–48. https://doi.org/10.1088/1361-6560/aa5bc7.
[14] Marquez-Mata CA, Mata Chavez MJ, Campillo-Rivera GE, Vazquez-Bañuelos J, Garcia-Duran A, Vega-Carrillo HR. Shielding features of seven types on natural quartz. Appl Radiat Isot 2021;167:109450. https://doi.org/10.1016/j.apradiso.2020.109450.
[15] Kavaz E, El_Agawany FI, Tekin HO, Perişanoğlu U, Rammah YS. Nuclear radiation shielding using barium borosilicate glass ceramics. J Phys Chem Solids 2020;142:109437. https://doi.org/10.1016/j.jpcs.2020.109437.
[16] Siva Sesha Reddy A, Lakshminarayana G, Purnachand N, Ravi Kumar V, Venkatramaiah N, Ravi Kumar V, Veeraiah N. Influence of gold ions on visible and NIR luminescence features of Er3+ ions in lead boroselenate glass ceramics. J Lumin 2020;226:117481. https://doi.org/10.1016/j.jlumin.2020.117481.
[17] Mann KS, Mann SS. Py-MLBUF: Development of an online-platform for gamma-ray shielding calculations and investigations. Ann Nucl Energy 2021;150:107845. https://doi.org/10.1016/j.anucene.2020.107845.
[18] RSICC Computer Code Collection. MCNPX User's Manual Version 2.4.0. Monte Carlo N-Particle Transport Code System for Multiple and High Energy Applications. 2002.
[19] Zakaly HMH, Saudi HA, Issa SAM, Rashad M, Elazaka AI, Tekin HO, Saddeek YB. Alteration of optical, structural, mechanical durability and nuclear radiation attenuation properties of barium borosilicate glasses through BaO reinforcement: Experimental and numerical analyses. Ceram Int 2021;47(4):5587–96. https://doi.org/10.1016/j.ceramint.2020.10.143.
[20] Kaur P, Singh D, Singh T. Heavy metal oxide glasses as gamma rays shielding material. Nucl Eng Des 2016;307:364–76. https://doi.org/10.1016/j.nucengdes.2016.07.029.
[21] Tekin HO, Sayyed MI, Issa SAM. Gamma radiation shielding properties of the hematite-serpentine concrete blended with WO3 and Bi2O3 micro and nano particles using MCNPX code. Radiat Phys Chem 2018;150:95–100. https://doi.org/10.1016/j.radphyschem.2018.05.002.
[22] Tekin HO, Singh VP, Manici T. Effects of micro-sized and nano-sized WO 3 on mass attenauation coefficients of concrete by using MCNPX code. Appl Radiat Isot 2017;121:122–5. https://doi.org/10.1016/j.apradiso.2016.12.040.
[23] Mostafa AMA, Zakaly HMH, Pyshkina M, Issa SAM, Tekin HO, Sidek HAA, Matori KA, Zaid MHM. Multi-objective optimization strategies for radiation shielding performance of BZBB glasses using Bi2O3: A FLUKA Monte Carlo code calculations. J Mater Res Technol 2020;9(6):12335–45. https://doi.org/10.1016/j.jmrt.2020.08.077.
[24] Tekin HO, Issa SAM, Kavaz E, Altunsoy Guclu EE. The direct effect of Er 2 O 3 on bismuth barium telluro borate glasses for nuclear security applications. Mater Res Express 2019;6:115212. https://doi.org/10.1088/2053-1591/ab4cb5.
[25] Al-Buriahi MS, Tekin HO, Kavaz E, Tonguc BT, Rammah YS. New transparent rare earth glasses for radiation protection applications. Appl. Phys. A 2019;125(12). https://doi.org/10.1007/s00339-019-3077-8.
[26] Sallam OI, Madbouly AM, Elalaily NA, Ezz-Eldin FM. Physical properties and radiation shielding parameters of bismuth borate glasses doped transition metals. J Alloy Compd 2020;843:156056. https://doi.org/10.1016/j.jallcom.2020.156056.
[27] Henaish AMA, El-Sharkawy AN, Shama SA, Hemeda OM, Ghazy R. Structure and optical properties of nano Nix Cd1-x Fe2O4 doped with optical dyes. J. Phys. Conf. Ser., vol. 1253, Institute of Physics Publishing; 2019. https://doi.org/10.1088/1742-6596/1253/1/012024.
[28] Mostafa AMA, Issa SAM, Zakaly HMH, Zaid MHM, Tekin HO, Matori KA, Sidek HAA, Elsaman R. The influence of heavy elements on the ionizing radiation shielding efficiency and elastic properties of some tellurite glasses: Theoretical investigation. Results Phys 2020;19:103496. https://doi.org/10.1016/j.rinp.2020.103496.
[29] Rashad M, Tekin HO, Zakaly HMH, Pyshkina M, Issa SAM, Susoy G. Physical and nuclear shielding properties of newly synthesized magnesium oxide and zinc oxide nanoparticles. Nuclear Engineering and Technology 2020;52(9):2078–84. https://doi.org/10.1016/j.net.2020.02.013.
[30] Issa SAM, Kassab LRP, Susoy G, Nishimura MVM, da Silva Mattos GR, Bordon CDS, Tekin HO. Fabrication, optical characteristic, and nuclear radiation shielding properties of newly synthesised PbO–GeO2 glasses. Appl. Phys. A 2020;126(9). https://doi.org/10.1007/s00339-020-03928-1.
[31] Kilic G, Issa SAM, Ilik E, Kilicoglu O, Issever UG, El-Mallawany R, Issa B, Tekin HO. Physical, thermal, optical, structural and nuclear radiation shielding properties of Sm2O3 reinforced borotellurite glasses. Ceram Int 2021;47(5):6154–68. https://doi.org/10.1016/j.ceramint.2020.10.194.
[32] Tekin HO, Kaçal MR, Issa SAM, Polat H, Susoy G, Akman F, Kilicoglu O, Gillette VH. Sodium dodecatungstophosphate hydrate-filled polymer composites for nuclear radiation shielding. Mater Chem Phys 2020;256:123667. https://doi.org/10.1016/j.matchemphys.2020.123667.
[33] Kara U, Susoy G, Issa SAM, Elshami W, Yorgun NY, Abuzaid MM, Kavaz E, Tekin HO. Iron (III) oxide doped lithium borate glasses: structural and charged particles/photon shielding properties. J Non-Cryst Solids 2020;546:120281. https://doi.org/10.1016/j.jnoncrysol.2020.120281.
[34] Divina R, Naseer KA, Marimuthu K, Alajerami YSM, Al-Buriahi MS. Effect of different modifier oxides on the synthesis, structural, optical, and gamma/beta shielding properties of bismuth lead borate glasses doped with europium. J Mater Sci: Mater Electron 2020;31(23):21486–501. https://doi.org/10.1007/s10854-020-04662-3.
[35] AlBuriahi MS, Hegazy HH, Alresheedi F, Olarinoye IO, Algarni H, Tekin HO, Saudi HA. Effect of CdO addition on photon, electron, and neutron attenuation properties of boro-tellurite glasses. Ceram Int 2021;47(5):5951–8. https://doi.org/10.1016/j.ceramint.2020.10.168.
[36] Lakshminarayana G, Kumar A, Tekin HO, Issa SAM, Al-Buriahi MS, Lee D-E, Yoon J, Park T. Binary B2O3–Bi2O3 glasses: scrutinization of directly and indirectly ionizing radiations shielding abilities. J Mater Res Technol 2020;9(6):14549–67. https://doi.org/10.1016/j.jmrt.2020.10.019.
[37] Stalin S, Gaikwad DK, Al-Buriahi MS, Srinivasu Ch, Ahmed SA, Tekin HO, Rahman S. Influence of Bi2O3/WO3 substitution on the optical, mechanical, chemical durability and gamma ray shielding properties of lithium-borate glasses. Ceram Int 2021;47(4):5286–99. https://doi.org/10.1016/j.ceramint.2020.10.109.
[38] Al-Buriahi MS, Somaily HH, Alalawi A, Alraddadi S. Polarizability, Optical Basicity, and Photon Attenuation Properties of Ag2O–MoO3–V2O5–TeO2 Glasses: The Role of Silver Oxide. J Inorg Organomet Polym 2021;31(3):1047–56. https://doi.org/10.1007/s10904-020-01750-z.
[39] Al-Buriahi MS, Alajerami YSM, Abouhaswa AS, Alalawi A, Nutaro T, Tonguc B. Effect of chromium oxide on the physical, optical, and radiation shielding properties of lead sodium borate glasses. J Non-Cryst Solids 2020;544:120171. https://doi.org/10.1016/j.jnoncrysol.2020.120171.
[40] Zakaly HMH, Rashad M, Tekin HO, Saudi HA, Issa SAM, Henaish AMA. Synthesis, optical, structural and physical properties of newly developed dolomite reinforced borate glasses for nuclear radiation shielding utilizations: An experimental and simulation study. Opt Mater 2021;114:110942. https://doi.org/10.1016/j.optmat.2021.110942.
[41] Abouhaswa AS, Mhareb MHA, Alalawi A, Al-Buriahi MS. Physical, structural, optical, and radiation shielding properties of B2O3- 20Bi2O3- 20Na2O2- Sb2O3 glasses: Role of Sb2O3. J Non-Cryst Solids 2020;543:120130. https://doi.org/10.1016/j.jnoncrysol.2020.120130.
[42] Naseer KA, Marimuthu K, Al-Buriahi MS, Alalawi A, Tekin HO. Influence of Bi2O3 concentration on barium-telluro-borate glasses: Physical, structural and radiation-shielding properties. Ceram Int 2021;47(1):329–40. https://doi.org/10.1016/j.ceramint.2020.08.138.
[43] Boukhris I, Kebaili I, Al-Buriahi MS, Alalawi A, Abouhaswa AS, Tonguc B. Photon and electron attenuation parameters of phosphate and borate bioactive glasses by using Geant4 simulations. Ceram Int 2020;46(15):24435–42. https://doi.org/10.1016/j.ceramint.2020.06.226.
[44] El-Taher A, Zakaly HM, Pyshkina M, Allam E, El-Sharkawy R, Mahmoud M, et al. A comparative Study Between Fluka and Microshield Modeling Calculations to study the Radiation-Shielding of Nanoparticles and Plastic Waste composites. Zeitschrift Für Anorg Und Allg. zaac.202100062 Chemie 2021. https://doi.org/10.1002/zaac.202100062.
[45] Al-Buriahi MS, Bakhsh EM, Tonguc B, Khan SB. Mechanical and radiation shielding properties of tellurite glasses doped with ZnO and NiO. Ceram Int 2020;46(11):19078–83. https://doi.org/10.1016/j.ceramint.2020.04.240.